

Supplementary Information

Structural basis for prostaglandin and drug transport via SLCO2A1.

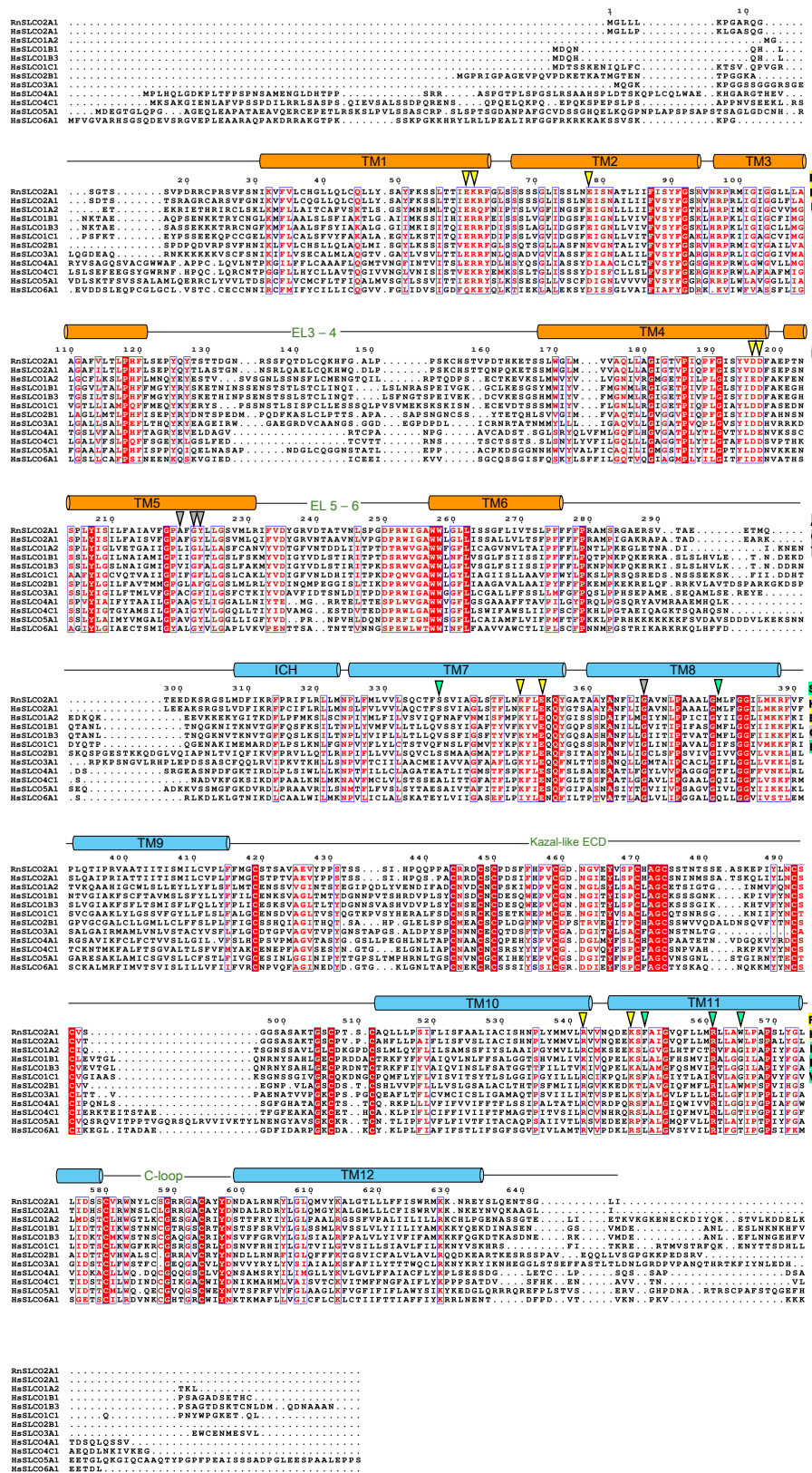
Chitra Joshi, Justin C Deme, Yoshinobu Nakamura, Wei-Tse Hsu *et al.*

*Corresponding author. Email: simon.newstead@bioch.ox.ac.uk

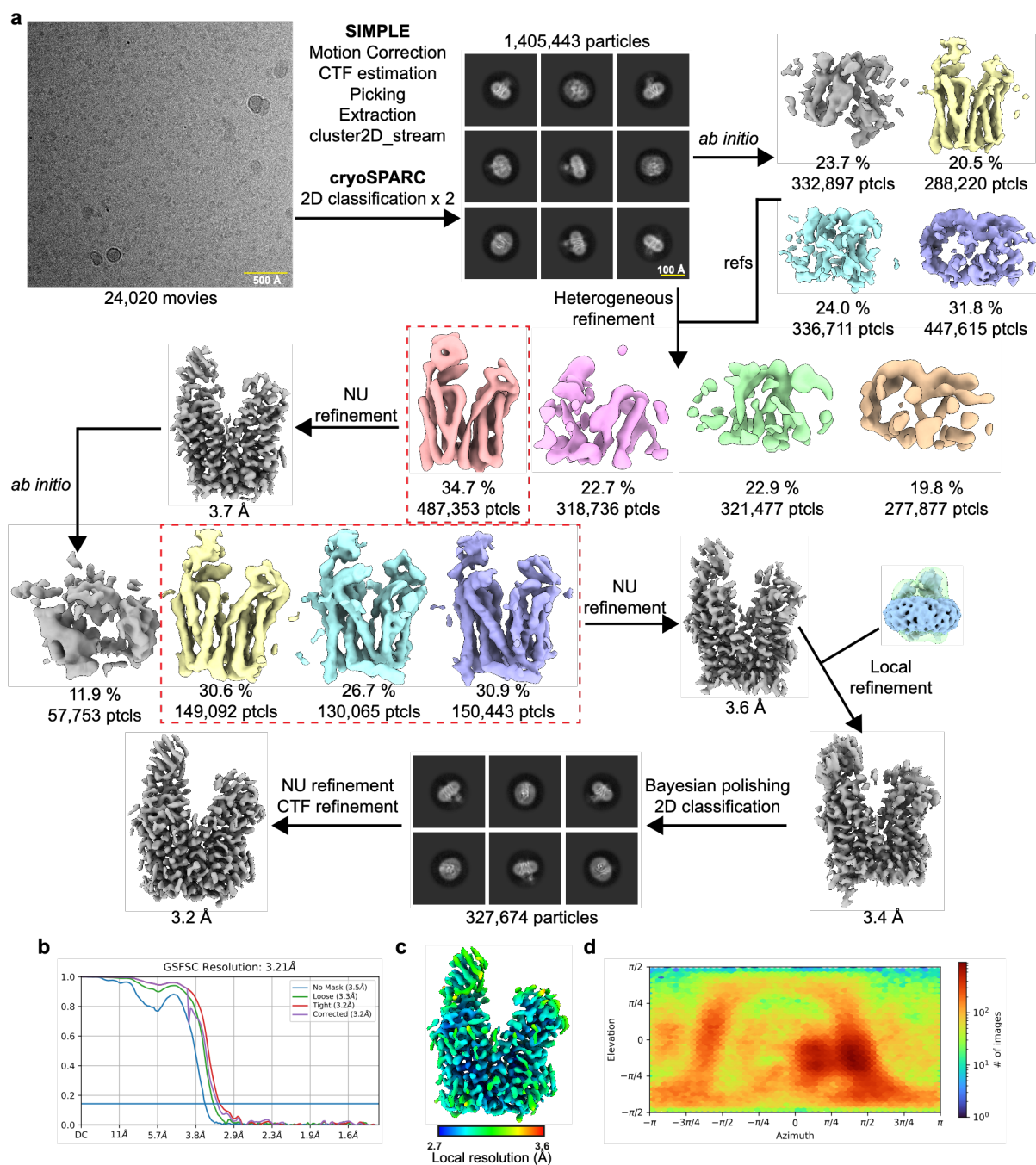
Supplementary Table 1. Cryo-EM data collection, refinement and validation statistics

	Slco2a1 Apo (PDB 9QZO) (EMD-53472)	Slco2a1 Prostaglandin E ₂ (PDB 9R0M) (EMD- 53484)	Slco2a1 Prostaglandin F _{2α} (PDB 9R0N) (EMD-53485)	Slco2a1 Tolcapone (PDB 9R0O) (EMD- 53486)
Data collection and processing				
Magnification	×165,000	×165,000	×165,000	×165,000
Voltage (kV)	300	300	300	300
Electron exposure (e−/Å ²)	61.2	60.3	55.0	55.0
Defocus range (μm)	-2.0 to -0.5	-2.0 to -0.5	-2.0 to -0.5	-2.0 to -0.5
Pixel size (Å)	0.732	0.732	0.732	0.732
Symmetry imposed	C1	C1	C1	C1
Initial particle images (no.)	16,180,538	11,250,696	9,949,417	12,435,376
Final particle images (no.)	220,549	327,674	206,784	131,095
Map resolution (Å)	2.9	3.2	3.4	3.1
FSC threshold	0.143	0.143	0.143	0.143
Map resolution range (Å)	2.5-16.0	2.7-25.7	2.9-19.6	2.7-48.8
Refinement				
Initial model used (PDB code)	AF-Q00910-F1			
Model composition in the asymmetric unit				
Non-hydrogen atoms	4266 550	4291 550	4287 549	4328 558
Protein residues	1	2	2	1
Ligands ^a				
Average B factors (Å ²)				
Protein	62.90	41.58	42.61	57.73
Ligand	20.00	44.56	30.28	71.24
R.m.s. deviations				
Bond lengths (Å)	0.003	0.004	0.004	0.003
Bond angles (°)	0.538	0.554	0.580	0.543
Validation				
MolProbity score	1.48	1.47	1.48	1.15
Clashscore	5.00	3.93	5.45	3.56
Poor rotamers (%)	1.93	1.71	1.07	0.42
Ramachandran plot				
Favored (%)	99.08	97.43	97.05	98.19
Allowed (%)	0.92	2.57	2.95	1.81
Outlier (%)	0.00	0.00	0.00	0.00

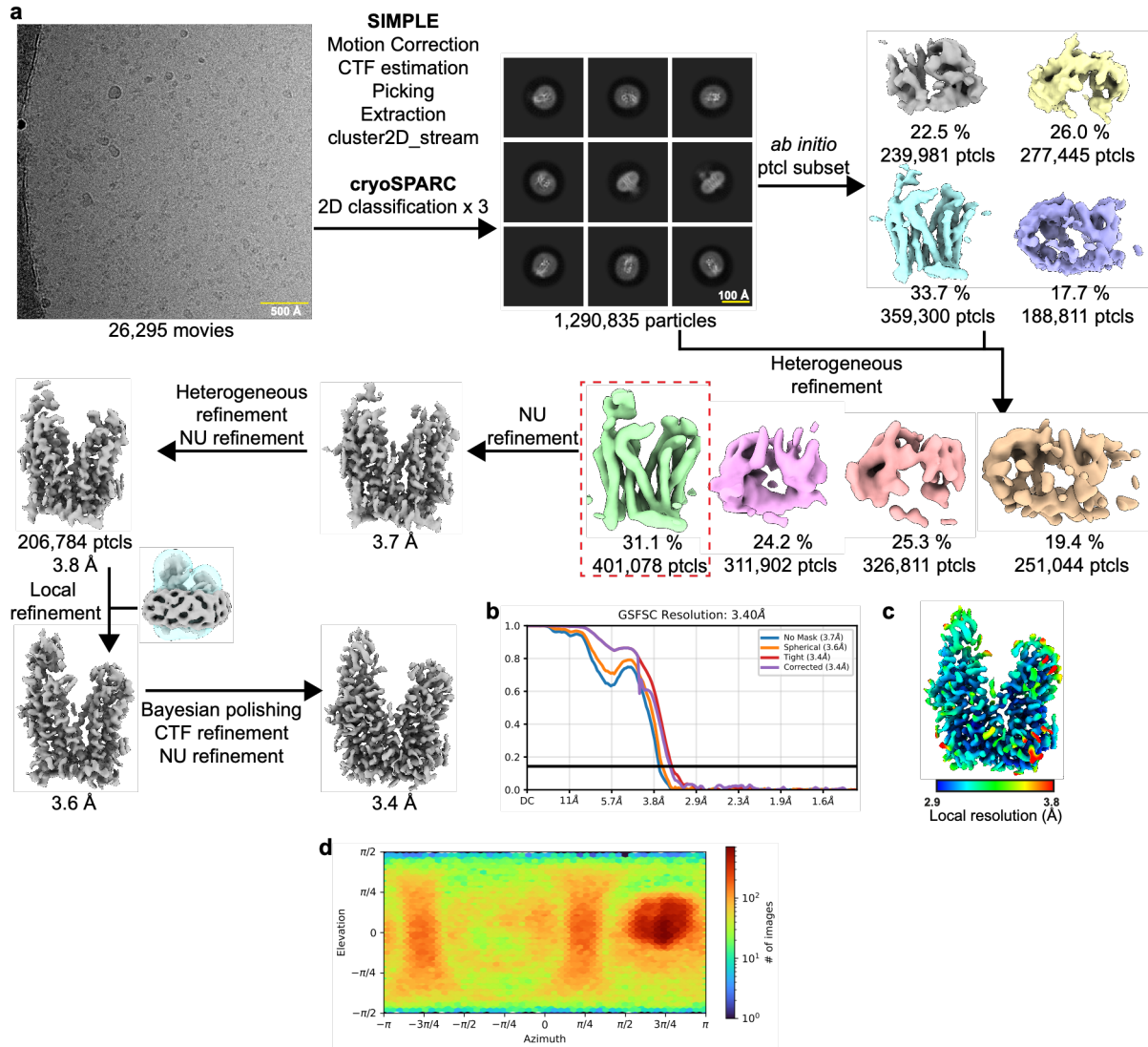
	Slco2a1 Fentiazac	Slco2a1 z Zafirlukast	Slco2a1 Losartan
	(PDB 9R0A) (EMD- 53482)	(PDB 9R07) (EMD-53481)	(PDB 9R0I) (EMD- 53483)
Data collection and processing			
Magnification	×105,000	×105,000	×105,000
Voltage (kV)	300	300	300
Electron exposure (e- /Å ²)	40.2	32.8	39.8
Defocus range (μm)	-2.4 to -1.0	-2.4 to -1.0	-2.4 to -1.0
Pixel size (Å)	0.832	0.832	0.832
Symmetry imposed	C1	C1	C1
Initial particle images (no.)	6,788,854	11,211,159	19,422,430
Final particle images (no.)	54,096	146,876	80,622
Map resolution (Å)	3.1	3.2	3.1
FSC threshold	0.143	0.143	0.143
Map resolution range (Å)	2.66-17.8	2.66-8.8	2.7-8.7
Refinement			
Initial model used (PDB code)	AF-Q00910-F1		
Model composition in the asymmetric unit			
Non-hydrogen atoms	4416	4425	4261
Protein residues	561	565	550
Ligands ^a	2	2	1
Average B factors (Å ²)			
Protein	85.41	58.01	88.61
Ligand	71.79	54.81	92.63
R.m.s. deviations			
Bond lengths (Å)	0.004	0.004	0.003
Bond angles (°)	0.548	0.990	0.481
Validation			
MolProbity score	1.33	1.39	1.19
Clashscore	4.84	3.25	4.08
Poor rotamers (%)	1.26	1.88	0.21
Ramachandran plot			
Favored (%)	98.20	97.67	98.71
Allowed (%)	1.80	2.33	1.29
Outlier (%)	0.00	0.00	0.00



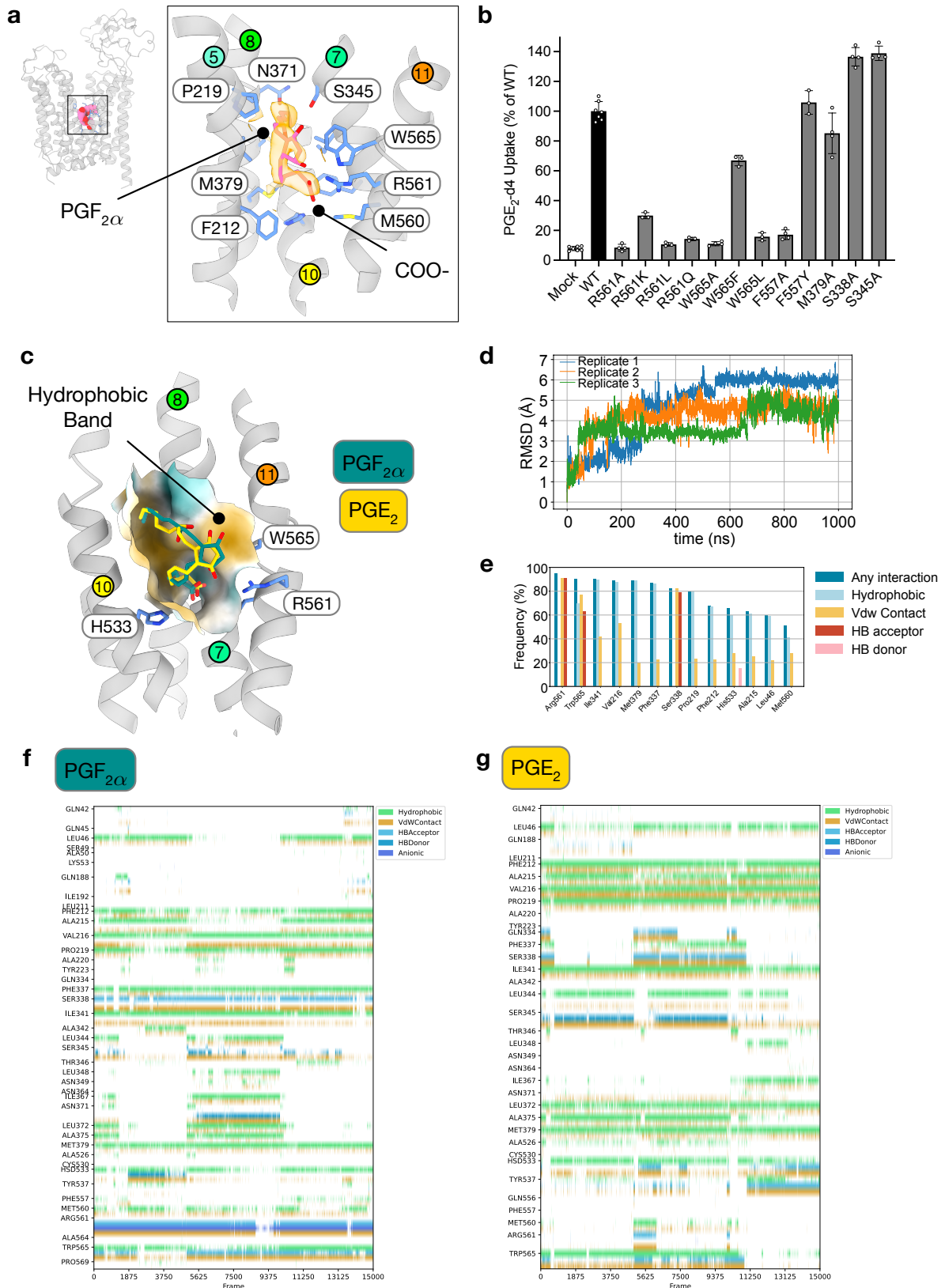
Supplementary Fig. 1: Sequence alignment of SLCO family members. N-terminal bundle TMs are coloured orange, and the C-terminal bundle is coloured blue. Structural annotation made based on rat Sloc2a1 cryo-EM structure. Key functionally essential residues are highlighted: green - PG recognition, yellow - salt bridge interacting residues and grey - lipid interacting residues.



Supplementary Fig. 2: Cryo-EM processing workflow for rat Slco2a1 with bound prostaglandin E2, including local and global resolution estimates. a, Image processing workflow, including representative cryo-EM micrograph at -2.0 μm defocus. **b**, Gold-standard Fourier Shell Correlation (FSC) curves used for global resolution estimation. **c**, Local resolution estimate of the volume. **d**, orientation distribution plot.

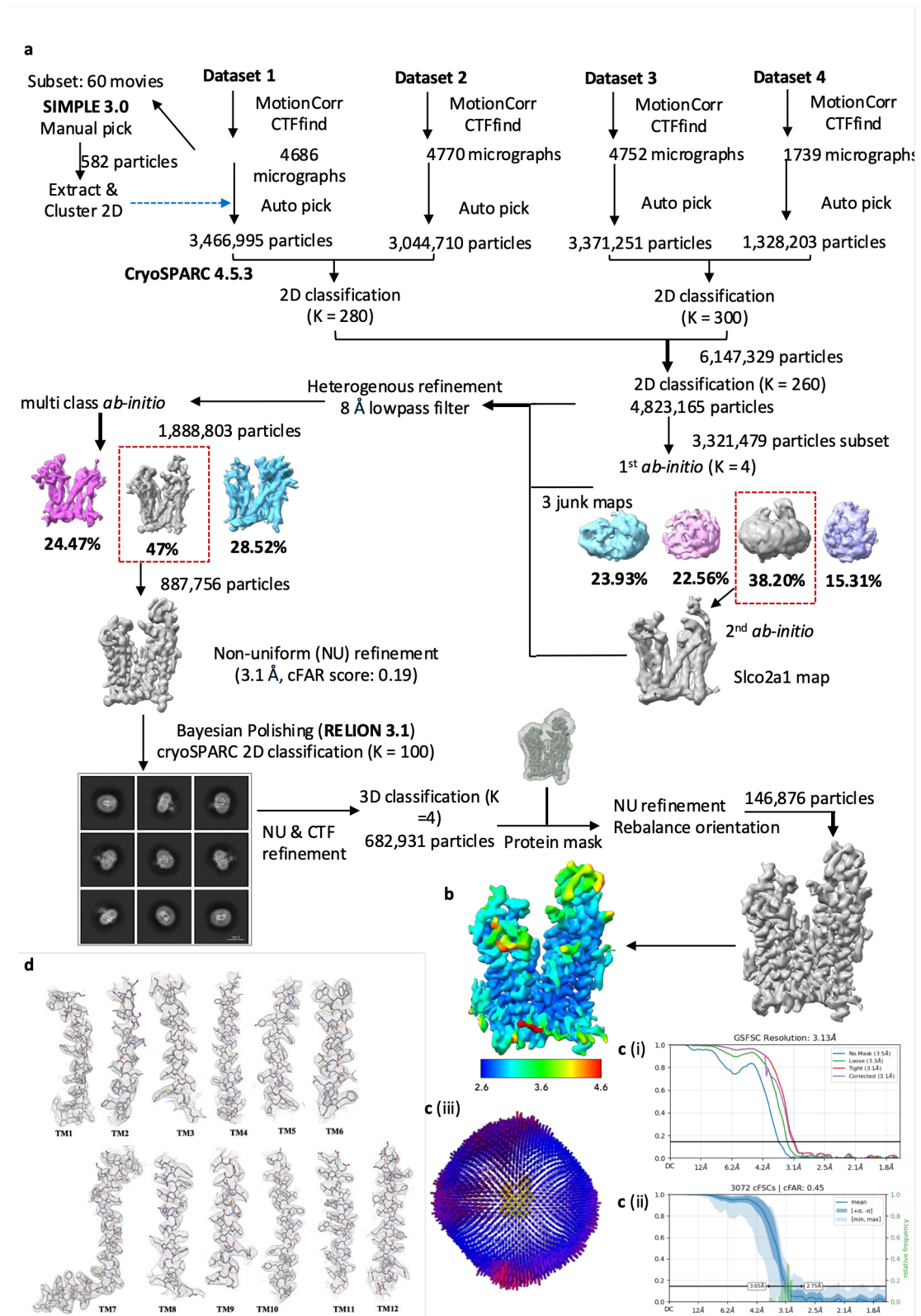


Supplementary Fig. 3: Cryo-EM processing workflow for rat Slco2a1 with bound PGF_{2α}, including local and global resolution estimates. a, Image processing workflow, including representative cryo-EM micrograph at -2.0 μm defocus. **b**, Gold-standard Fourier Shell Correlation (FSC) curves used for global resolution estimation. **c**, Local resolution estimate of the volume. **d**, orientation distribution plot.



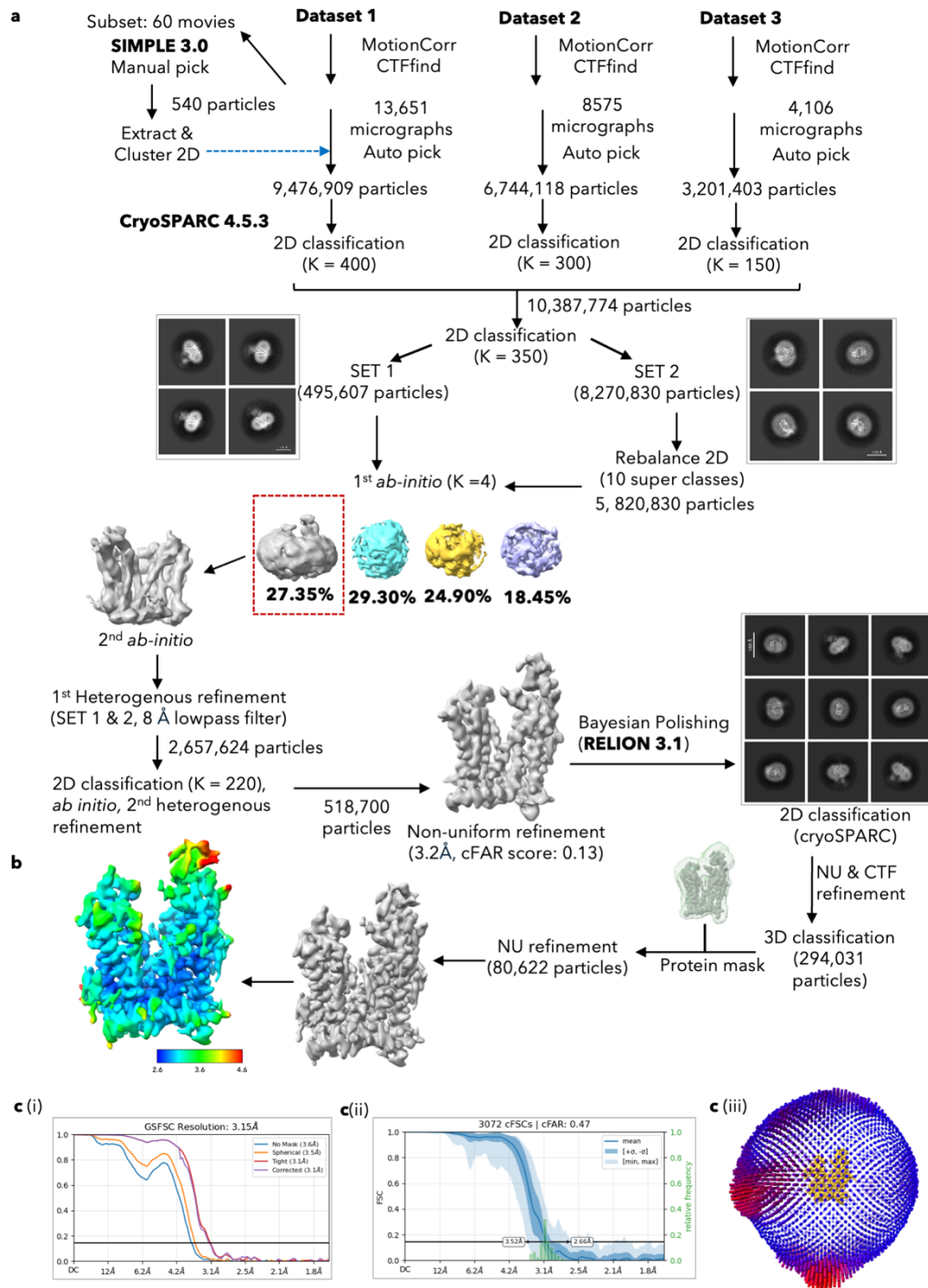
Supplementary Fig. 4: Cryo-EM structure of rat Slco2a1 bound to PGF_{2α}. **a**, The Cryo-EM structure of rat Slco2a1 showing the location of the bound PGF_{2α} ligand (PDB: 9R0N). **Inset-right:** zoomed-in view of the binding site, revealing the main interactions formed with PGF_{2α}. Key residues that interact with or are near the substrate are displayed as sticks. Cryo-

EM volume density for PGF_{2α} is shown (orange and threshold 0.13). **b**, Cell-based transport assays for PGE₂ in wild type (WT) and mutant rat Slco2a1. n = 7 independent experiments for the WT and the mock-transfected control, and n = 3 (R561K; R561L; R561Q; W565F; W565L; F557Y); n = 4 (R561A; W565A; F557A; M379A; S338A; S345A); data shown are the mean and error bars are s.d. **c**, Structural overlay of the PGF_{2α} and PGE₂ (PDB: 9R0M) structures with the surface coloured by hydrophobicity. **d**, 2D plot showing ligand-aligned r.m.s.d of the PGF_{2α} position in three replicates of the 1μs simulation. **e**, 2D plot showing the frequency of different types of interactions observed for residues that interacted with the ligand in more than 50% of the simulation frames. Results were calculated from the trajectory pooled across all three replicates. **f**, Time series plots of the PGF_{2α} interactions with Slco2a1. **g**, Time series plots of the PGE₂ interactions with Slco2a1.



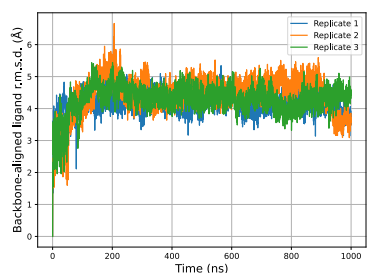
Supplementary Fig. 5: Cryo-EM processing workflow for rat Slco2a1 with bound Zafirlukast, including local and global resolution estimates. a, Image processing workflow for Slco2a1 with zafirlukast. **b**, Local-resolution estimate of the volume. **c (i)**, Gold-standard Fourier Shell Correlation (FSC) curves used for global resolution estimation. **c (ii)**, Conical FSC area ratio (cfar) curve. **c (iii)**, Angular distribution histogram of volume. **d**, Close-up view

of maps and side-chain density for transmembrane helices. Volume contoured at a threshold level of 0.25.

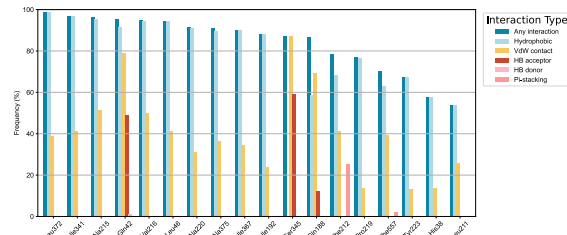


Supplementary Fig. 6: Cryo-EM processing workflow for rat Slco2a1 with bound Losartan, including local and global resolution estimates. a, Image processing workflow for Slco2a1 with Losartan. **b**, Local-resolution estimate of the volume. **c (i)**, Gold-standard Fourier Shell Correlation (FSC) curves used for global resolution estimation. **c (ii)**, Conical FSC area ratio (cfar) curve. **c (iii)**, Angular distribution histogram.

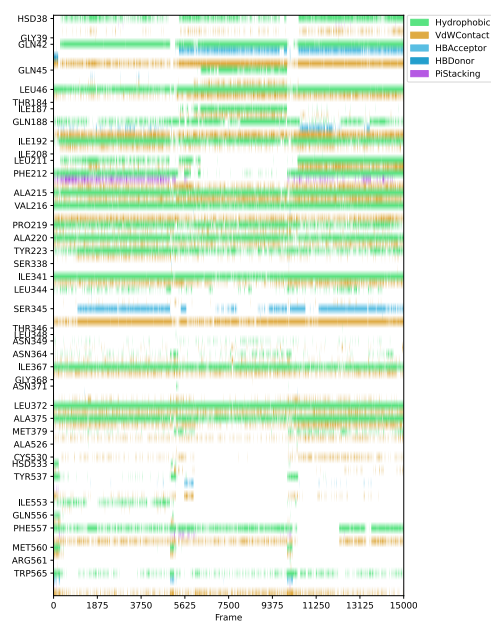
a Zafirlukast



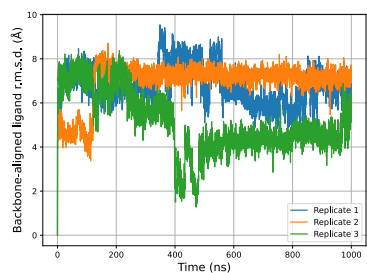
b



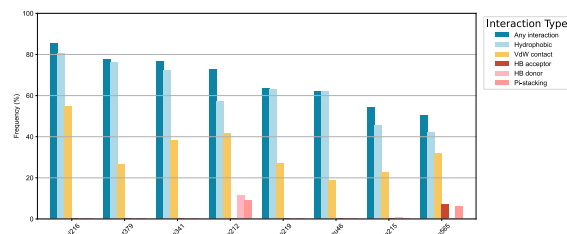
c



d Losartan



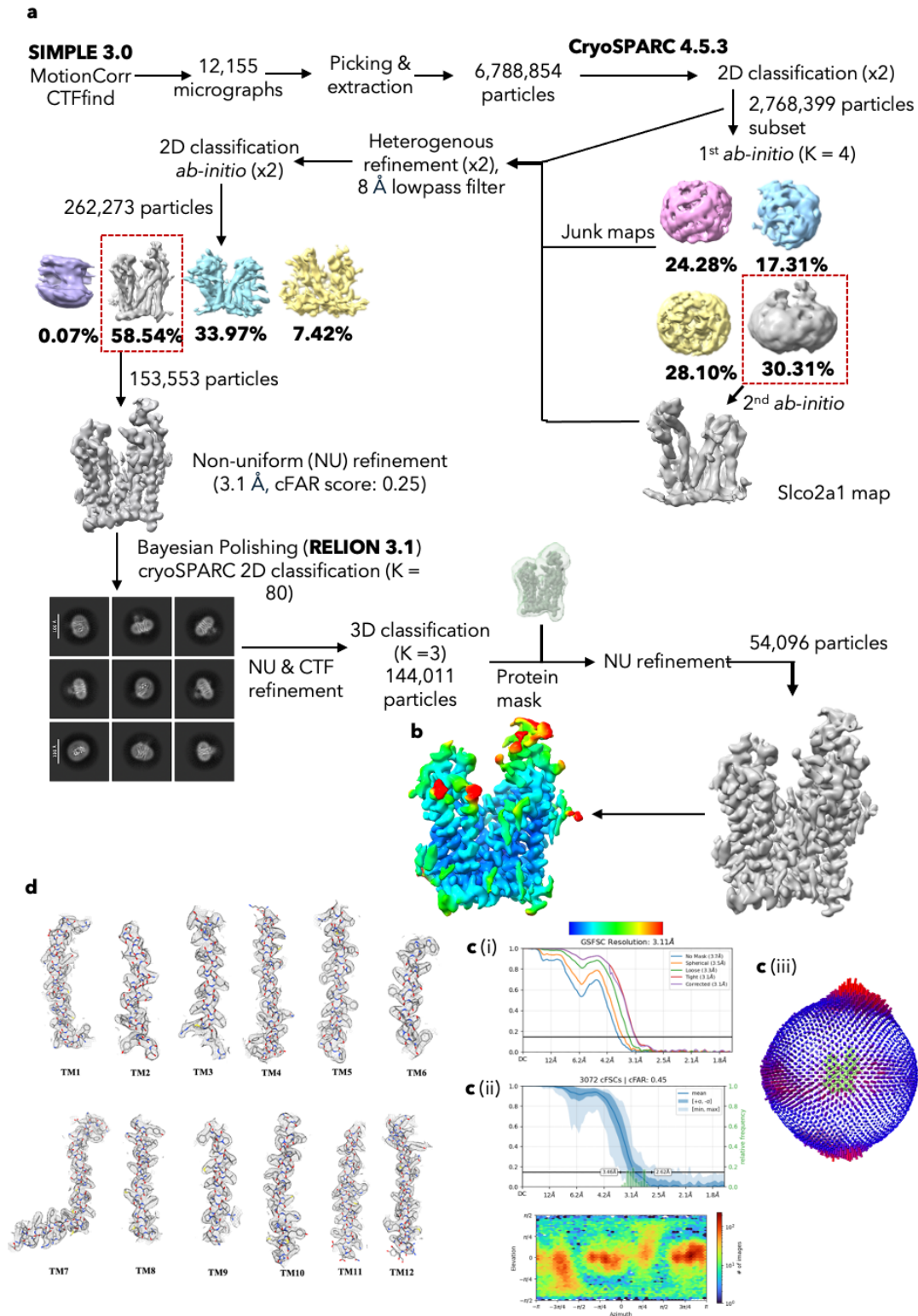
e



f

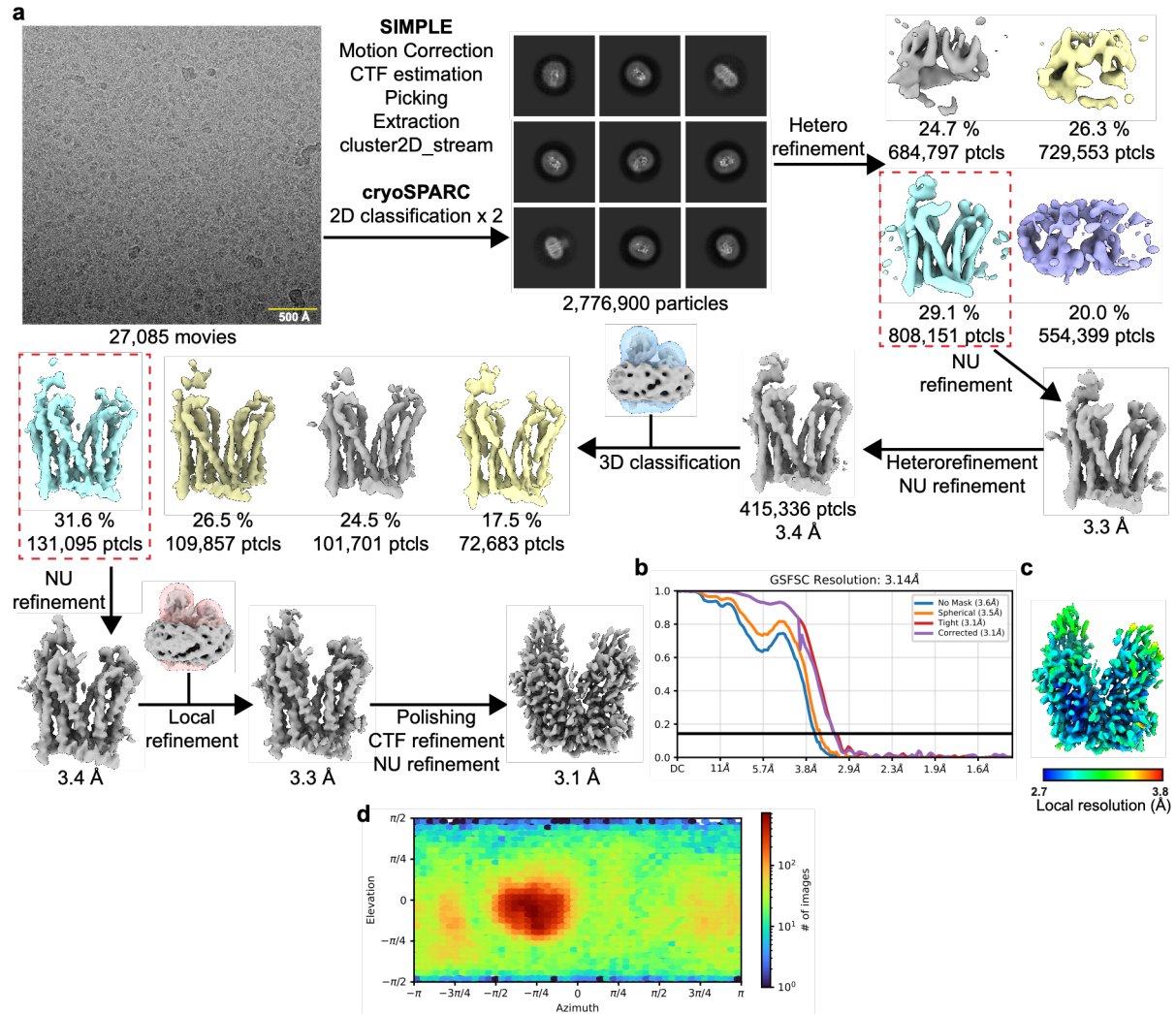


Supplementary Fig. 7: Molecular dynamics analysis of Zafirlukast and Losartan interactions. **a**, 2D plot showing ligand-aligned r.m.s.d of the Zafirlukast position in three replicates of the 1 μ s simulation. **b**, 2D plot showing the frequency of different types of interactions observed in more than 50% of the simulation frames. Results were calculated from the trajectory pooled across all three replicates. **c**, Time series plots of the interactions made to Zafirlukast. **d**, 2D plot showing ligand-aligned r.m.s.d of the Tolcapone position in three replicates of the 1 μ s simulation. **e**, 2D plot showing the frequency of different types of interactions observed in more than 50% of the simulation frames. Results were calculated from the trajectory pooled across all three replicates. **f**, Time series plots of the interactions made to Tolcapone.

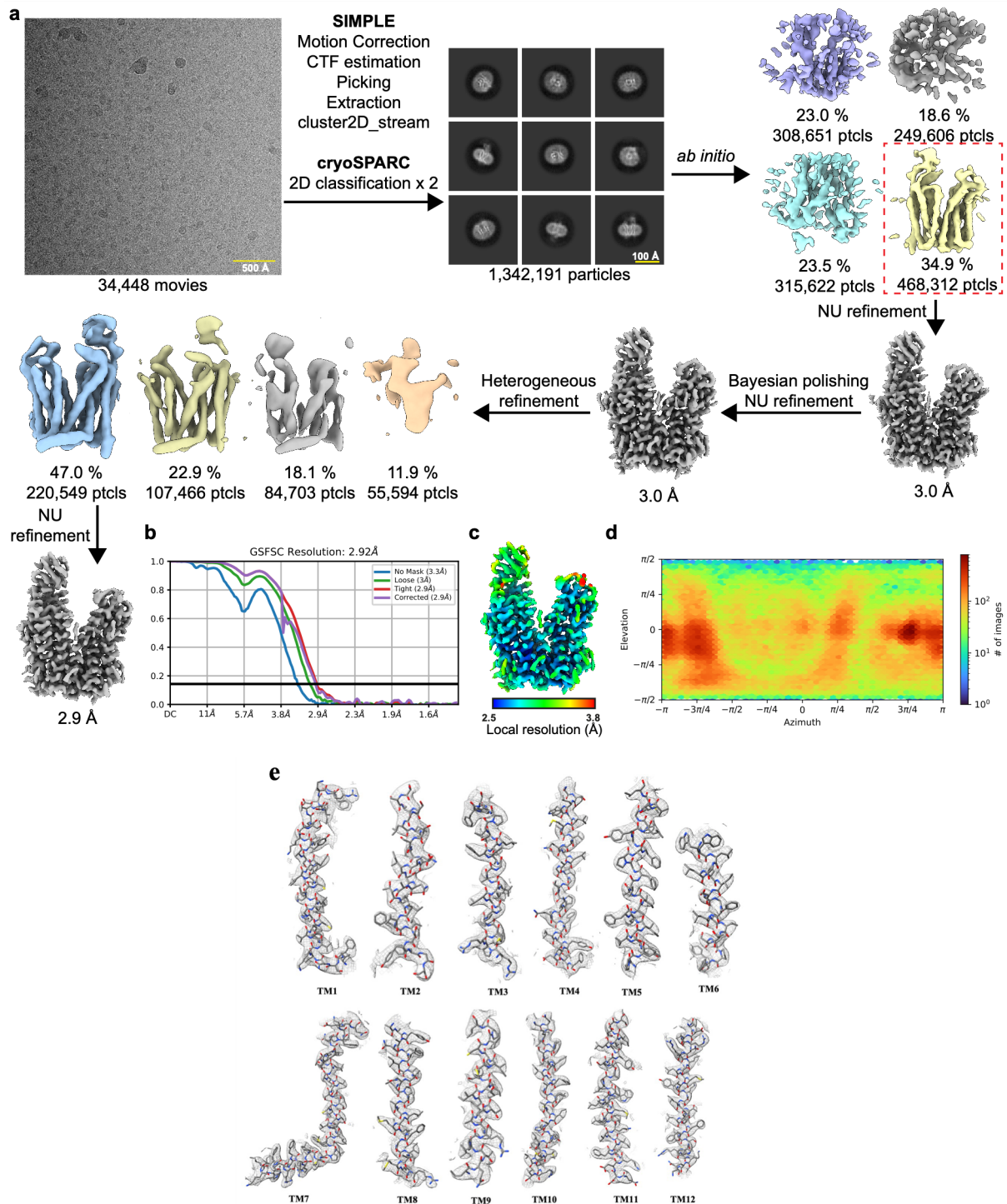


Supplementary Fig. 8: Cryo-EM processing workflow for rat Slco2a1 with bound Fentiazac, including local and global resolution estimates. a, Image processing workflow for Slco2a1 with Losartan. **b**, Local-resolution estimate of the volume. **c (i)**, Gold-standard Fourier Shell Correlation (FSC) curves used for global resolution estimation. **c (ii)**, Conical FSC area ratio (cfar) curve. **c (iii)**, Angular distribution histogram. **d**, Close-up view of maps

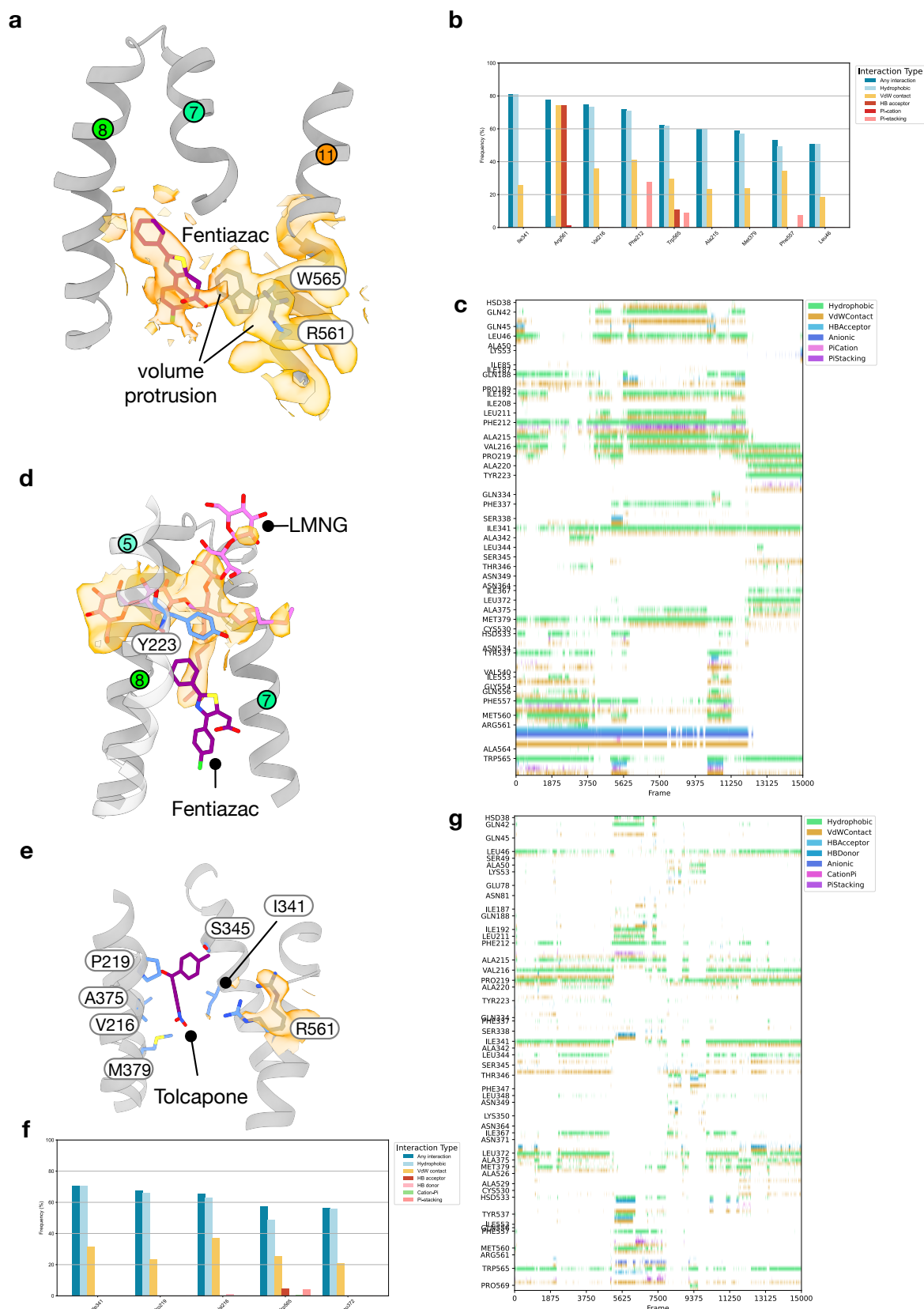
and side-chain density for transmembrane helices. Volume contoured at a threshold level of 0.25.



Supplementary Fig. 9: Cryo-EM processing workflow for rat Slco2a1 with bound Tolcapone, including local and global resolution estimates. a, Image processing workflow, including representative cryo-EM micrograph at -2.0 μm defocus. **b**, Gold-standard Fourier Shell Correlation (FSC) curves used for global resolution estimation. **c**, Local resolution estimate of the volume. **d**, Orientation distribution plot.

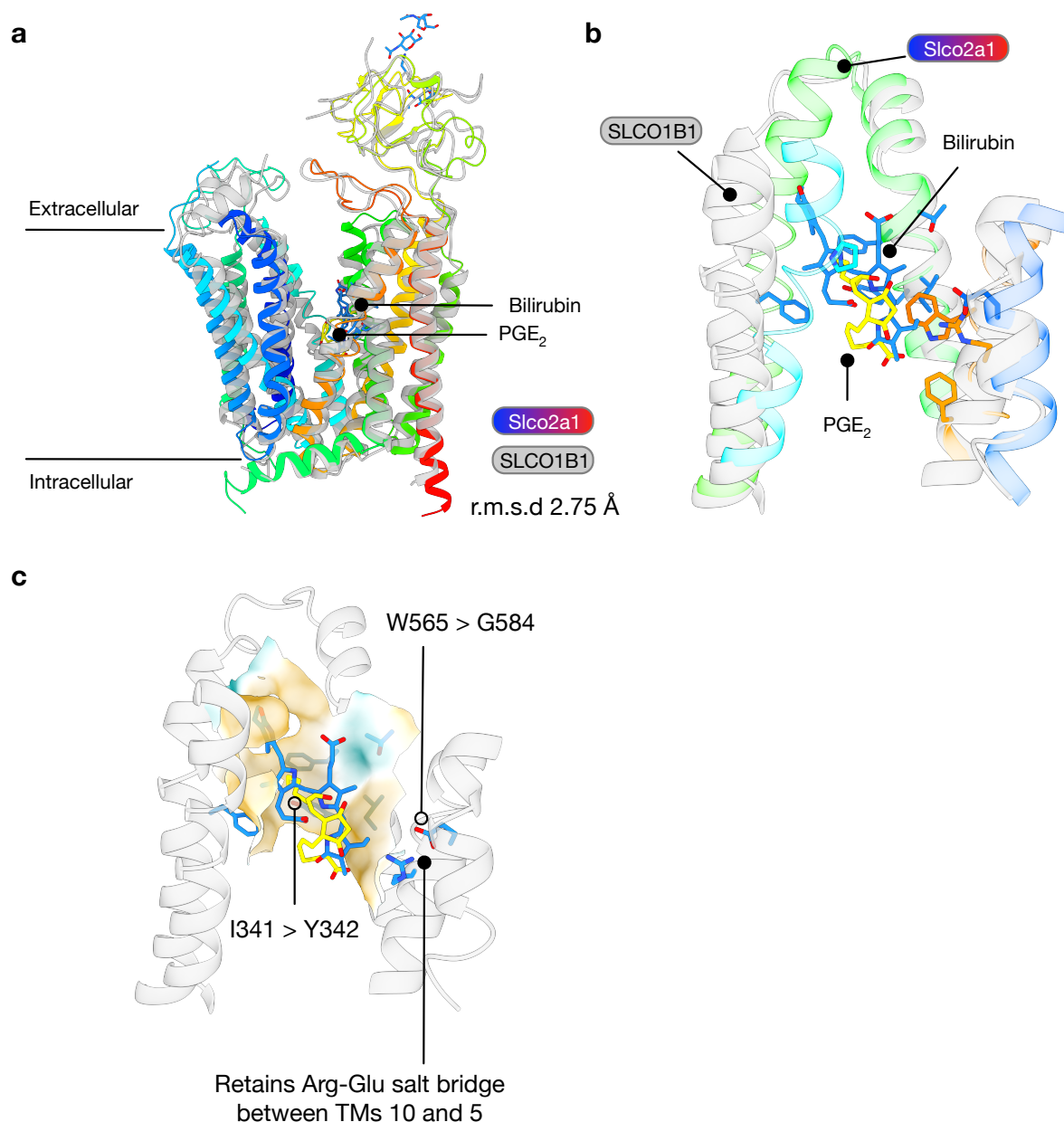


Supplementary Fig. 10: Cryo-EM processing workflow for apo rat Slco2a1, including local and global resolution estimates. **a**, Image processing workflow, including representative cryo-EM micrograph at -2.0 μm defocus. **b**, Gold-standard Fourier Shell Correlation (FSC) curves used for global resolution estimation. **c**, Local resolution estimate of the volume. **d**, orientation distribution plot. **e**, Close-up view of maps and side-chain density for transmembrane helices. Volume contoured at a threshold level of 0.25.



Supplementary Fig. 11: Inhibitor binding in rat *Slco2a1*. **a**, A close-up view of the bound Fentiazac drug (magenta). Cryo-EM volume density is depicted (orange and threshold 0.7). **b**, 2D plot showing the frequency of different types of interactions observed for residues that

interacted with Fentiazac in more than 50% of the simulation frames. Results were calculated from the trajectory pooled across all three replicates. **c**, Time series plots of the interactions made to Fentiazac within the binding site of Slco2a1. **d**, A close-up view of the bound LMNG detergent molecule (pink). Cryo-EM volume density is depicted (orange and threshold 0.56). **e**, A close-up view of the bound Tolcapone drug (purple). Cryo-EM volume density is depicted (orange and threshold 0.25). **f**, 2D plot showing the frequency of different types of interactions observed for residues that interacted with Tolcapone in more than 50% of the simulation frames. Results were calculated from the trajectory pooled across all three replicates. **g**, Time series plots of the interactions made to Tolcapone.



Supplementary Fig. 12: Structural comparison of rat Slco2a1 with human SLCO1B1 (OATP1B3). **a**, Superimposed structures of the PGE₂-bound Slco2a1 (PDB: 9R0M) and bilirubin-bound SLCO1B1 (PDB: 8HNC). The 8HNC model was chosen as the transporter is in the same conformational state as SLCO2A1. The substrates are shown as sticks and labelled. **b**, A zoomed-in view of the binding sites in both proteins highlights the interacting side chains. Helices and side chains in Slco2a1 are coloured according to Jones' rainbow, while helices in SLCO1B1 are coloured dark grey, and side chains are coloured cornflower blue. **c**, An equivalent view to that shown in **b**, where the surface of SLCO1B1 is coloured based on hydrophobicity, and key residue differences from Slco2a1 are indicated.